The Huygens Doppler Wind Experiment

M. K. Bird,[1] M. Heyl,[1] M. Allison,[2] S. W. Asmar,[3] D. H. Atkinson,[4] P. Edenhofer,[5] D. Plettemeier,[5] R. Wohlmuth,[5] L. Iess[6] & G. L. Tyler[7]

[1]*Radioastronomisches Institut, Universität Bonn, Auf dem Hügel 71, D-53121 Bonn, Germany*
E-mail: mbird@astro.uni-bonn.de Fax: +49 228 73 3672
[2]*NASA Goddard Institute for Space Studies, New York, NY 10025, USA*
[3]*NASA Jet Propulsion Laboratory, California Institute of Technology, Pasadena, CA 91109, USA*
[4]*Department of Electrical Engineering, University of Idaho, Moscow, ID 83843, USA*
[5]*Institut für HF-Technik, Universität Bochum, D-44780 Bochum, Germany*
[6]*Dipartimento Aerospaziale, Universitá di Roma 'La Sapienza', I-00184 Rome, Italy*
[7]*Center for Radar Astronomy, Stanford University, Stanford, CA 94305, USA*

The primary scientific objective of the Doppler Wind Experiment is to determine the direction and strength of Titan's zonal winds. A height profile of wind velocity will be derived from the residual Doppler shift of the Probe's radio relay signal to the Cassini Orbiter, corrected for all known orbit and propagation effects. Wind-induced motion of the Probe will be measured to a precision better than 1 m/s from parachute deployment at an altitude of ~160 km down to the surface. As secondary objectives, this investigation is also capable of providing valuable information on Probe dynamics (e.g. spin rate and spin phase) during the atmospheric descent, as well as the Probe's location and orientation up to and after impact on Titan.

1. Introduction

The Doppler Wind Experiment (DWE) is a high-precision tracking investigation to determine wind direction and magnitudes in Titan's atmosphere. The prime science objective, a height profile of the wind velocity, will be derived from the Doppler shift of the Probe Relay Link (PRL) signal from the Huygens Probe to the Cassini Orbiter. After correcting for all known Doppler shifts due to orbit and propagation effects, the wind-induced motion of the Probe will be determined to an accuracy of better than 1 m/s, from parachute deployment at an altitude of ~160 km down to surface impact.

In addition to the measurements of drift motions due to winds, DWE is capable of achieving two secondary scientific objectives:

(a) measurement of Doppler fluctuations to determine the level and spectral index of turbulence and possible wave activity in Titan's atmosphere
(b) measurement of Doppler and signal level modulation to monitor Probe descent dynamics, including its rotation rate and phase, parachute swing and post-impact status.

By achieving the first of these objectives, DWE will contribute, along with Probe accelerometry and radio occultation measurements, to the assessment of atmospheric turbulence associated with vertical wave propagation, the buoyantly-driven surface layer or possible methane moist convection.

The second objective represents a potential DWE 'service' to other Probe instruments to assist in the interpretation of their data. The known Probe-Orbiter

geometry enables a determination of directions on Titan from the phase of the Doppler/amplitude modulation. The Probe's passively-controlled spin rate will also be determined to a high degree of accuracy from the same data. These precise measurements of velocity will be integrated to reconstruct the descent flight path, thereby providing the most accurate determination of the Probe's impact coordinates.

The most severe constraints on the accuracy of the DWE wind measurement are trajectory errors and instability of the Probe oscillator used to generate the PRL signal. Present assessments of these limitations indicate that a zonal wind height profile $u(z)$ can be recovered with a mean error δu of less than ± 1 m/s. This can be achieved only with a sufficiently stable PRL signal over the duration of the descent ($\delta f \lesssim 0.4$ Hz at S-band) in order to exclude contamination of the measurement by oscillator drift. The transmitter's frequency stability is guaranteed by using an ultrastable oscillator (USO) to generate the PRL carrier signal. In addition to this transmitter USO (TUSO), it is necessary to incorporate an additional unit in the receiver (RUSO) of the Probe Support Avionics (PSA) on the Cassini Orbiter, where the frequency measurement is recorded.

Current theories of Titan's winds and some comments on DWE synergism with other ground-based and Cassini/Huygens investigations are presented in the next section. Following this, we describe the investigation's methodology and outline the recovery algorithm for retrieving the zonal wind profile from the PRL frequency measurements. The paper concludes with a description of the DWE-instrumentation, the TUSO/RUSO ultrastable oscillators and their associated development programme.

2. The Winds of Titan

2.1 Expectations based on Voyager results

Almost all presently available information about Titan's atmospheric dynamics and meteorology derives from Voyager 1's reconnaissance, with essential contributions from the infrared interferometry spectrometer (IRIS) and radio occultation (RSS) investigations (Hanel et al., 1981; Tyler et al., 1981).

Titan's vertical temperature-pressure structure, retrieved from Voyager RSS data (Lindal et al., 1983), is represented by the profile shown in Fig. 1. The occultation data

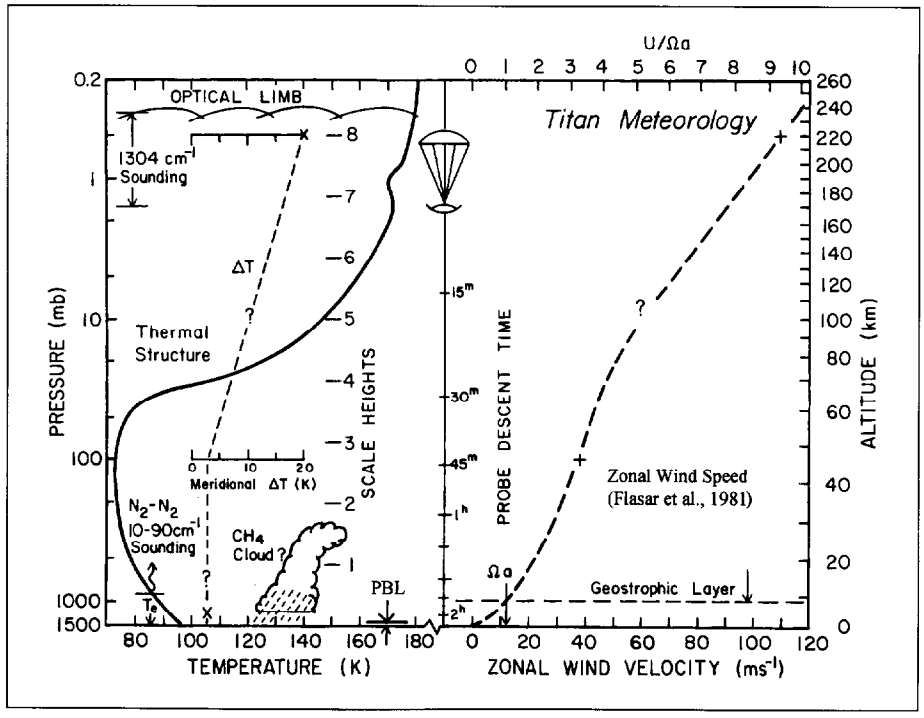

Fig. 1. Titan meteorology. The vertical thermal structure retrieved from Voyager radio science data (Lindal et al., 1983) is represented by the solid-line temperature profile $T(P)$ in the left panel. The equator-to-pole temperature contrast, as extrapolated from Voyager IRIS data (Flasar et al., 1981), is represented by the dashed-line profile referred to the inset scale. The dashed curve in the right-hand panel is the corresponding mid-latitude wind profile inferred from the vertical integration of the thermal wind equation, assuming vanishing velocity at the surface. The nominal descent time scale of the Huygens Probe is indicated in the middle of the figure.

extend all the way to the surface, where the temperature is approximately 97K (with a systematic uncertainty of about ±7K). Methane clouds may form above a few kilometres, depending on the relative humidity near the surface (Toon et al., 1988). The decrease of temperature with altitude below 40 km implies the absorption of sunlight at the surface and a weak tropospheric greenhouse. The radio occultation measurements indicate a nearly adiabatic lapse rate below 3-4 km, consistent with the inferred turbulent surface layer, but a statically stable profile above this height. Hinson & Tyler (1983) have found evidence for vertically propagating gravity waves at altitudes of 25-90 km, based on their analysis of radio occultation scintillations.

The indirect inference of 100 m/s zonal cyclostrophic winds on Titan is based primarily upon the latitudinal contrast of temperature at infrared sounding levels observed by Voyager's IRIS (Flasar et al., 1981; Flasar & Conrath, 1990). As interpreted by the thermal wind equation under the assumption of hydrostatic gradient-balanced flow, the vertical variation of the Coriolis plus centripetal acceleration of the zonal velocity u is related to the latitudinal temperature gradient $\partial T/\partial\lambda$ by

$$\frac{\partial}{\partial \hat{z}} [u^2 \tan \lambda + 2u\Omega a \sin \lambda] = -R \frac{\partial}{\partial \lambda} \left[\frac{T}{\mu} \right] \qquad (1)$$

where $\hat{z} = \ln(P_0/P)$ is the vertical log-pressure coordinate with P_0 the surface pressure, λ the latitude, a the planetary radius, Ω the planetary rotation velocity, μ the mean molecular weight (mass per mole) of the atmospheric gas, and R the gas constant. With the further plausible assumption of relatively weak winds near the surface (cf. Allison, 1992), the thermal wind equation may be solved for the zonal velocity at all levels for which there are vertically continuous observations of the horizontal temperature gradient. The second term in the thermal wind equation (1) can be neglected, except very close to the surface, because of the slow Titan angular rotation. The resulting circulation is in cyclostrophic balance with $\Omega a/u \ll 1$. However, the direction of the zonal wind (prograde or retrograde) cannot be uniquely determined from (1) under this condition.

The vertical integration of the thermal wind equation for the practical inference of zonal motions requires the independent specification of the velocity at one or more levels where the thermal gradient can be accurately estimated. For sufficiently strong surface drag, the zonal velocity at the bottom of the atmosphere may be assumed to be nearly zero. On this basis, and assuming an equator-to-pole temperature contrast given by the dashed line in the inset (left panel) of Fig. 1, Flasar et al. (1981) estimated a zonal wind as depicted schematically in Fig. 1 (dashed line in right panel), approaching 100 m/s in the upper stratosphere at a latitude of $\lambda = 45°$.

Although Titan's thermal spectrum is partly convolved with variable aerosol opacity, the 1304 cm^{-1} region, which comes mainly from the 0.5 mbar pressure level (~230 km), is presumed to be relatively free of these effects. Measured brightness variations across the disc in this channel could thus be interpreted as a real difference in kinetic temperature between low and high latitudes of roughly 16K (Flasar et al., 1981). More recently, Flasar & Conrath (1990) retrieved stratospheric temperatures from a combination of the measured radiances at 1304 cm^{-1} and the P and Q branches of methane at 1260-1292 cm^{-1}, essentially confirming the results of the earlier brightness temperature analysis. The data also indicated a hemispheric asymmetry in Titan's latitudinal temperature distribution at the time of the Voyager encounters. Coustenis (1991) has performed an independent retrieval of the latitudinal temperature structure as inferred from the 1304 cm^{-1} channel, with similar results. IRIS measurements for a second thermal sounding channel at 200 cm^{-1}, corresponding to emission in the vicinity of 100 mbar (~40 km), suggest that latitudinal thermal contrasts at this level may be less than about 1K. Measurements for a third thermal

channel at 530 cm^{-1}, corresponding to emission near Titan's surface, were interpreted by Flasar et al. (1981) as a latitudinal temperature difference of about 2K between the equator and 60° latitude. This interpretation has since been qualified, however, by the study of Toon et al. (1988), who pointed out that stratospheric aerosols may also contribute significantly to the brightness temperature at this wavenumber. The apparent latitudinal contrast may thus be best interpreted as a crude upper limit to actual variations in the kinetic temperature. A more comprehensive review of the evidence supporting our contemporary model of Titan's zonal winds has been compiled by Flasar et al. (1997).

As with Venus, the inferred cyclostrophic flow regime on Titan is not yet understood, representing a fundamental unresolved problem in the theory of atmospheric dynamics. The magnitudes of the meridional and vertical winds are also quite speculative. Assuming the poleward advection of heat is balanced by radiative cooling, Flasar et al. (1981) estimated a mean meridional motion of $v \leq 0.04$ cm/s in the lower troposphere. Invoking continuity, the associated mean vertical motion may be estimated as $\omega \sim vH/a \leq 10^{-3}$ cm/s, where $H \approx 20$ km is the pressure scale height. It is possible that much stronger vertical motions exist in locally turbulent regions of the atmosphere, such as a methane thunderhead, but probably only over a relatively small fraction of the total area. The associated depth of the Ekman planetary boundary layer (PBL in Fig. 1), where the surface winds are rotated and strongly sheared with altitude until they match the thermal wind aloft, may be estimated as $D_E \approx 0.7$ km (Allison, 1992). Because the PBL mediates the transfer of angular momentum from the surface to the atmosphere, it is an important target for observational characterisation. With strong surface drag and a global meridional thermal contrast no larger than assumed by Flasar et al. (1981), the vertically integrated thermal wind equation implies a geostrophic regime ($\Omega a/u \gg 1$) extending up to about 5 km altitude.

In view of the various gaps and uncertainties in the thermal structure data, we cannot claim to know very much about the vertical and horizontal structure of Titan's zonal wind. Assuming that at least the 1304 cm^{-1} measurements from Voyager's IRIS have been more or less correctly interpreted, however, it is difficult to escape the conclusion that the thermal wind balance will involve zonal motions of the order of $(R\Delta T/\mu)^{1/2} \approx$ 70 m/s at stratospheric levels. The direct observational confirmation of the inferred zonal cyclostrophic motion of Titan's atmosphere by DWE will represent a fundamental contribution to the study of planetary meteorology. If its conjectured analogy to Venus is established, it would imply the probable ubiquity of atmospheric superrotation as a robust feature of slowly rotating, differentially heated planets.

2.2 Atmospheric model simulations

Only recently has a general circulation model (GCM), originally developed for the simulation of the terrestrial weather and climate, begun to be adapted successfully to the study of atmospheric superrotation on Titan. Del Genio et al. (1993) have shown that the addition of an optically thick, statically stable upper cloud layer to a terrestrial GCM, also modified with a 16-day planetary rotation period, results in the generation of an equilibrated zonal-mean flow of several tens of metres per second. Their diagnosis of the responsible flux transports indicate that this regime is supported by the horizontal mixing of quasi-barotropic eddies. Similar results have also been obtained with a Titan GCM under development by Hourdin et al. (1995). Despite their preliminary state of development, these GCM experiments lend some confidence to the indirect inference of superrotational winds from the observations.

Allison et al. (1994) have argued that the GCM experiments as well as the limited planetary observations are suggestive of the dynamical maintenance of these circulations by efficient 'potential vorticity' mixing. In the implied 'ZPV' (zero potential vorticity) limit for stable zonal flow, the latitudinal wind profile will be

bounded by a maximum envelope of the form

$$U_{max} = (U_e + \Omega a)(\cos \lambda)^{(2/R_i)-1} - \Omega a \cos \lambda \qquad (2)$$

where R_i is the local Richardson number (the squared ratio of the Brunt-Vaisala frequency to the vertical wind shear), and U_e is the zonal velocity at the equator. Except where R_i is less than 2, this envelope implies an increase in the maximum possible velocity with latitude, and can therefore be expected to approximate the actual winds only between the equator and the latitudes of the 'jet' maxima. The Titan zonal wind profile presented by Hubbard et al. (1993) is consistent with this prescribed envelope within 60° latitude, assuming a large value for the Richardson number, as appropriate for the statically stable stratosphere. The combination of the vertical wind shear measured by the Doppler Wind Experiment and the static stability inferred from the Huygens Atmospheric Structure Instrument (HASI) will provide an in situ determination for the vertical profile of R_i, which could then be interpreted with the ZPV constraint for comparison with independent remote sensing observations from the Cassini Orbiter.

2.3 Recent and future ground-based observations

Some independent evidence for winds on Titan, based on ground-based stellar occultation measurements, has been presented by Hubbard et al. (1993). Their analysis of the indicated latitudinal deformation of isopycnic surfaces in the stratosphere implies a zonal wind at the 0.25 mbar level varying from some 80 m/s near the equator to >170 m/s at 60° latitude. Another promising new method for determining stratospheric wind motions is the IR heterodyne observation of Titan's ethane emission at 841 cm^{-1}, which originates primarily from the 1 mbar level (T. Kostiuk, 1993, private communication). Initial measurements of the differential Doppler shift between east and west limb spectra indicate that the winds are *prograde* and have speeds of the order of 80 m/s.

Fifty near-IR Titan images were obtained with the Hubble Space Telescope's refurbished planetary camera (WF/PC2) during 4-18 October 1994 (Smith et al., 1994; Smith et al., 1996). A variety of continuum and methane filters were employed with the goal of obtaining cloud-tracked drift speeds associated with the differential motion of longitudinal structure of the type previously observed at 970 nm by Smith et al. (1992). A global surface map compiled from 14 processed images covering nearly the full Titan rotation period reveals a large bright feature in the leading hemisphere centred just south of the equator. Although some structure in the unaveraged images is suggestive of cloud features, attempts to derive cloud-tracked vectors have thus far proved unsuccessful. Further observations, obtained during Saturn's opposition of September/October 1995, are being evaluated (Caldwell et al., 1996).

The DWE will complement remote sensing observations of temperatures and winds from the Cassini Orbiter. It will provide ground-truth corroboration of the thermal wind retrievals from Composite Infrared Spectrometer (CIRS) measurements, also providing a check on their assumed aerosol and cloud opacities. The high vertical resolution of the DWE retrieval of vertical shear near impact will provide an important characterisation of the surface boundary layer unobtainable by thermal sounding. If the probe encounters sufficiently vigorous turbulence or vertical wave propagation, variations of the Doppler signal will provide information on the associated eddy momentum mixing and/or planetary waves.

3. DWE Concept and Mission Planning

3.1 Titan targeting

The geometrical configuration and sequence of events during descent are of vital importance to DWE's execution. The present mission baseline (Lebreton & Matson, 1997) plans Probe release on the Orbiter's first inbound pass after Saturn Orbit Insertion (SOI). The nominal date for Probe descent is 27 November 2004, some 150 days after SOI and >7 years after launch. Titan, which orbits Saturn at a constant distance of 20.4 Saturn radii, is very close to Saturn's noon meridian on this date.

Probe separation from the Orbiter occurs ~22 days before Titan encounter, at which point the Probe is targeted for entry into Titan's atmosphere. The final Orbiter Deflection Manoeuvre is performed 2 days after Probe separation, targeting the Orbiter so that it will fly very nearly over the Probe but at a safe 1500 km above Titan's surface. The Orbiter's closest approach is delayed to about 4 h after the Probe's atmospheric entry. This Orbiter Delay Time (ODT) is short enough to provide adequate margin of the PRL at the beginning of descent (maximum range) and yet long enough to avoid Orbiter High Gain Antenna (HGA) pointing problems toward the end of Huygens' mission (minimum range).

The Probe's target is characterised by parameters in Titan's *B-plane*, defined by the asymptotic Probe approach velocity as shown in Fig. 2. Aim points in the *B-plane* are defined by the magnitude of the impact parameter vector $\vec{B}$ and its associated azimuthal angle with respect to the *T-axis*. Equivalently, the atmospheric entry angle γ at a given altitude could be used instead of the impact parameter B. This alternative was adopted for Huygens mission planning purposes.

It is planned to target the Probe to the position shown in Fig. 3 at an entry angle $\gamma = 64°$, and *B-plane* azimuth angle $\theta = -60°$. The Probe delivery accuracy (3σ) in the *B-plane* is given by the ellipse encircling the tip of the target vector ($\theta = -60°$,

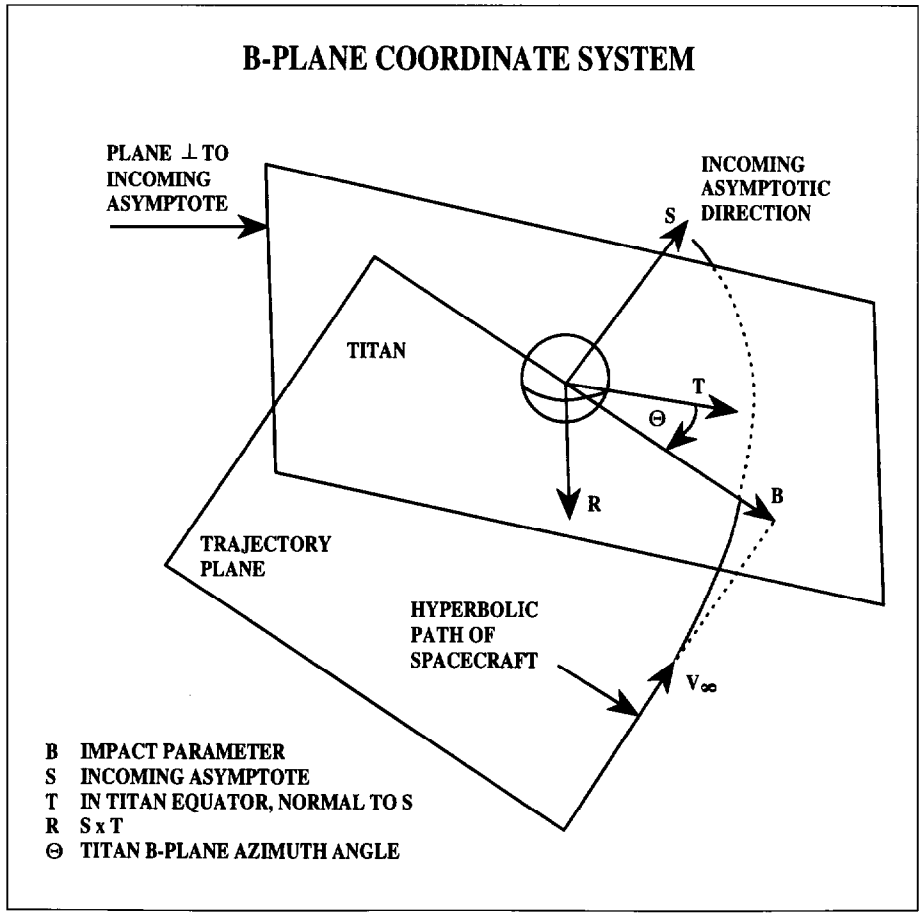

Fig. 2. Definition of the Titan *B-plane*. The normal to the *B-plane* (origin at Titan centre) is given by the direction of the asymptotic probe approach velocity $\vec{S}$. The intersection of this plane with Titan's equator defines the direction of the vector $\vec{T}$. *The vector* $\vec{R} = \vec{S} \times \vec{T}$, also lying in the *B-plane*, completes the 3-axis system.

$\gamma = 64°$) in Fig. 3. The semi-major and semi-minor axes of the ellipse are 452 km in the horizontal (longitudinal) direction and 59 km in the vertical (latitudinal), respectively. The targeted value of γ, defined as the angle between the nadir direction and the Probe's velocity vector at a reference height of 1270 km, was selected to ensure a safe atmospheric entry and to guarantee successful Probe radio communications via the PRL. Contours of constant γ are drawn as concentric dotted circles in Fig. 3. The Probe's targeted latitude is $\simeq 18°$N.

Owing to the extreme elongation of the error ellipse in the horizontal direction, dispersion in the entry angle is small for values of $\theta \simeq -90°$, but quite large for $\theta \simeq 0°$. In order to minimise entry angle dispersion, Huygens' *B-plane* target azimuth was selected as $\theta = -80°$ in the early stages of the mission planning process. Considerable trade-off analyses, however, were conducted to address scientific preferences for the impact latitude, solar zenith angle (SZA) and, specifically for DWE, the angle between the east-west direction on Titan and the line-of-sight direction from Probe to Orbiter. This angle, referred to as the Doppler Wind Component (DWC) angle, was very unfavourable to DWE for $\theta = -80°$. The cosine of the angle DWC, which is the 'zonal wind projection' (ZWP) onto the PRL ray path, regulates the magnitude of the Doppler shift from zonal winds. The nearly vertical solid curves in Fig. 3 are contours of constant ZWP.

A study of the DWE wind recovery algorithm under various Probe/Orbiter geometries showed that a very good representation of the input wind was derived for ZWP >0.5. This is shown as Region (a) in Fig. 3. Less precise, but still satisfactory, recoveries could be obtained in Region (b), where $0.3 < \text{ZWP} < 0.5$. The discrepancy between the input wind and the recovered profile begins to increase dramatically, however, when ZWP <0.3. The Region (c), where the zonal wind recovery error

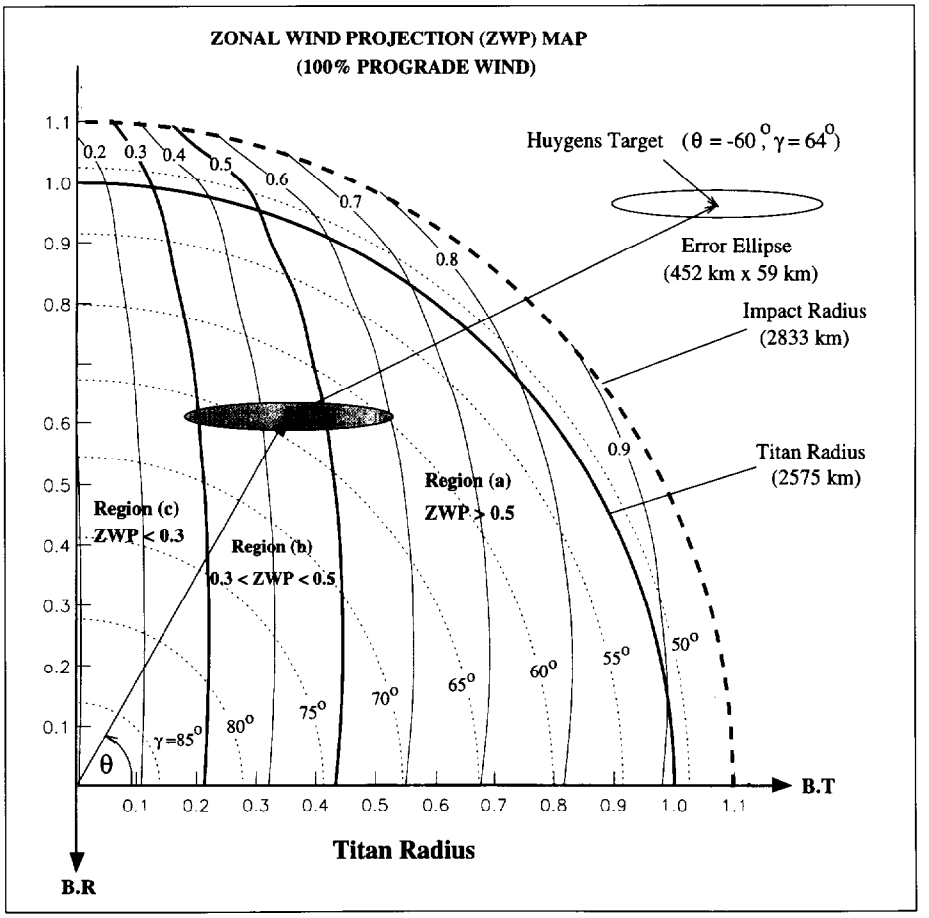

Fig. 3. Huygens' target in the upper right quadrant of the Titan *B-plane*.

became unacceptably large, was thus declared a 'zone of avoidance' by DWE.

The original Huygens target with $\gamma = 64°$, $\theta = -80°$ was, in fact, located in Region (c). The DWE request to move the *B-plane* azimuth angle to $\theta = -60°$ was granted after carefully reassessing the consequences for the overall mission performance. Only a very small portion of the 3σ targeting ellipse in Fig. 3 is now located in Region (c). The calculations of ZWP were performed for the '100% nominal' input wind model (prograde, linearly increasing from zero at the surface to 100 m/s at 200 km altitude; Flasar et al., 1981). Different contours are obtained for other wind models. A prograde zonal wind significantly shifts the touchdown site to the east of the Probe's atmospheric injection point, thereby improving the ZWP. The situation is the reverse for retrograde winds, which tend to increase the recovery errors. For all reasonable cases tested, however, the recovery algorithm never becomes indeterminate (i.e. when ZWP→0).

3.2 Titan atmospheric descent: PRL Doppler effects

As the Probe enters Titan's atmosphere, it is subjected to a severe deceleration at ~250 km altitude that could be as high as 16.1 g. A parachute is deployed near Mach 1.5, marking the beginning of the descent phase (time = t_0). After the Probe slows to subsonic velocity, the heat shield is jettisoned (at t_0+30 s) and the PRL is established for transmitting data to the Orbiter (no later than t_0+150 s). The large initial parachute is released at t_0 + 15 min and replaced by a smaller drogue in order to decrease the descent duration.

3.2.1 Probe motion during descent

The Probe's motion in Titan's atmosphere is determined by the action of two forces: gravity and wind drag. The acceleration due to wind drag $\vec{a}_d$ is taken from Flury (1986) to be:

$$\vec{a}_d = -\frac{\rho(z)}{2C_B} V_{PW} \vec{V}_{PW} \tag{3}$$

where $\rho(z)$ is the atmospheric density, $\vec{V}_{PW} = \vec{V}_P - \vec{V}_W$ is the relative velocity of the Probe with respect to the atmospheric wind, and C_B is the ballistic coefficient (units: kg/m^2) defined by:

$$C_B = \frac{m}{C_D A} \tag{4}$$

with m = probe mass, C_D = drag coefficient, and A = effective probe area to the flow.

The wind velocities in the (x, y, z) directions of a Cartesian coordinate system on Titan's surface are given by:

u = zonal wind	(x-axis: positive towards east)
v = meridional wind	(y-axis: positive towards north)
w = vertical wind	(z-axis: positive upwards)

The Probe's equation of motion during the Titan descent phase can thus be written:

$$\ddot{x} = -\frac{\rho}{2C_B} V_{PW} (\dot{x} - u) \tag{5}$$

$$\ddot{y} = -\frac{\rho}{2C_B} V_{PW} (\dot{y} - v) \tag{6}$$

$$\ddot{z} = -\frac{\rho}{2C_B} V_{PW} (\dot{z}-w) - g(z) \tag{7}$$

where $g(z)$ is Titan's gravitational acceleration, and

$$V_{PW} = [(\dot{x}-u)^2 + (\dot{y}-v)^2 + (\dot{z}-w)^2]^{1/2} \tag{8}$$

The meridional and vertical winds, v and w, are assumed to be considerably weaker than the zonal wind u. In this case, the latitude of the Probe (y component) remains approximately constant. Knowing the Probe's velocity on Titan, it is not difficult to determine the Doppler shift projected on to the PRL ray path back to the Orbiter:

$$\Delta f = -\frac{f}{c} \Delta V \tag{9}$$

where

$$\Delta V = (\vec{V}_P - \vec{V}_O) \cdot \vec{\Delta} \tag{10}$$

with $\vec{V}_P$ = Probe velocity wrt Titan centre
$\vec{V}_O$ = Orbiter velocity wrt Titan centre
$\vec{\Delta}$ = unit vector pointing from Orbiter to Probe

The vector $\vec{\Delta}$ defines the line-of-sight of the PRL. ΔV is negative during descent, so that the received frequency is increased (blue shifted). The PRL Doppler shift (9) is $\simeq 37.6$ kHz for the nominal Orbiter starting approach velocity of -5.53 km/s. The velocity of the Probe projected on to the line-of-sight can be written:

$$\vec{\Delta} \cdot \vec{V}_P = V_1 + V_2 + V_3 + V_4 \tag{11}$$

where

$$V_1 = \dot{x} \sin\alpha \cos\beta \tag{12}$$

$$V_2 = \Omega (a+z) \cos\lambda \sin\alpha \cos\beta \tag{13}$$

$$V_3 = \dot{y} \sin\alpha \sin\beta \tag{14}$$

$$V_4 = \dot{z} \cos\alpha \tag{15}$$

Furthermore, we define the projection of the Orbiter velocity on to the line-of-sight by:

$$\vec{\Delta} \cdot \vec{V}_O = V_5 \tag{16}$$

The angles α and β define the direction from the Probe to the Orbiter in a local Cartesian coordinate system on the Probe oriented along a natural Titan coordinate grid (x-axis positive towards east; y-axis positive towards north; z-axis positive upwards). The angle α, basically the zenith angle of the Orbiter as seen from the Probe (Ott, 1991), is also sometimes designated as the 'probe aspect angle' (PAA). The azimuthal angle β of the Probe-to-Orbiter line-of-sight is labelled the 'line-of-sight azimuth' (LOSA) by some authors (Atkinson, 1989; Pollack et al, 1992).

The term V_1 in (12), where the mean value of $\dot{x} \simeq u$, the drift velocity due to zonal winds, is the quantity to be determined by DWE. This velocity is co-aligned with the contribution V_2 in (13) due to Titan rotation. It is assumed for simulation purposes that the rotation is synchronous with Titan's orbital period ($\Omega a \simeq 11.7$ m/s). As noted in the previous section, the relative importance of V_1, and thus the quality of the reconstructed wind profile, is strongly dependent on the values of α and β.

The term V_3 in (14), arising from meridional drift, should be small because $\dot{y}$ is not

expected to be important. The term V_4 in (15) contains the vertical descent velocity $\dot{z}$. This quantity can be obtained to a high degree of accuracy either from the range rates deduced from the Probe's proximity sensor data, or using measurements of temperature T and pressure P from HASI. In the latter case, based on the assumption of hydrostatic equilibrium and ideal gas behaviour, the descent velocity is determined from:

$$\dot{z} = -\frac{H}{P}\frac{dP}{dt} \tag{17}$$

where variations in $H = RT/\mu g$, the atmospheric scale height, are assumed to be negligible over the altitude range of Huygens' descent. The final error associated with the determination of the reconstructed Probe descent velocity is estimated to be of the order of 1%.

Knowing $\dot{z}(t)$ from the proximity sensor or from HASI measurements, it is possible to reconstruct $\dot{x}(t) \approx u(t)$ from the PRL's Doppler shift (9). Using in situ measurements of the density $\rho(z)$, we can then extract the exact height profile $u(z)$ from the motion equations (5) and (7). Comparitive wind measurements are expected near the surface from two independent sources on board the Probe:

- proximity sensor measurements using pendulum swing motion, or
- inference of horizontal motion from the Descent Imager/Spectral Radiometer (DISR).

This would provide verification of the DWE height profile for the last few data points before touchdown, when horizontal winds are likely to be weak. If the Probe survives the surface impact and continues to transmit, further DWE measurements might provide a frequency reference for zero wind. The post-impact data are not necessarily a reliable calibration, however, because the Probe oscillator may execute shock-induced frequency shifting at impact.

In order to provide a rough estimate of the Doppler shifts involved, Fig. 4 shows the results of a simplified calculation of the five line-of-sight velocity contributions to the PRL frequency shift, V_1-V_5. The geometry for the calculations was taken from the nominal descent profile (duration: 135 min). The upper and lower panels show the same curves on different ordinate scales.

Only the *change* in the Orbiter's projected velocity from its initial value, $V_5(t)$-$V_5(0)$, is plotted in Fig. 4. The total projected velocity is plotted for the other contributions, all of which happen to be negative (blue shift in PRL frequency) in this example. The 100% nominal zonal wind model was used for computing the zonal wind contribution V_1. The Titan rotation term V_2 is almost constant during the entire descent. The meridional winds in V_3 were taken to be a constant +1 cm/s (blowing towards north). The change of parachutes at t = 15 min is clearly seen in the curve for V_4, which is the second largest contributer to the changing Doppler shift.

In addition to the derivation of a zonal wind height profile from the large-scale drift, DWE may be able to provide valuable science and navigation services from the small-scale variations in frequency as a by-product of the analysis. Two such possibilities are:

1. knowledge of the zonal wind velocity enables an extremely accurate reconstruction of the flight path during descent, and therefore the best possible determination of the impact coordinates on Titan
2. rotational motion of the Probe during descent will produce a small modulation in the PRL frequency and signal level that will be exploited to derive the Probe's spin rate and spin phase, thereby effectively serving as a compass in the Titan landscape.

The amplitude of the Doppler modulation from the rotation is proportional to the spin rate. The ultimate accuracy of the Doppler measurement, limited by the clock digitisation of the PSA receivers, is 60 mHz. This accuracy translates to an estimate

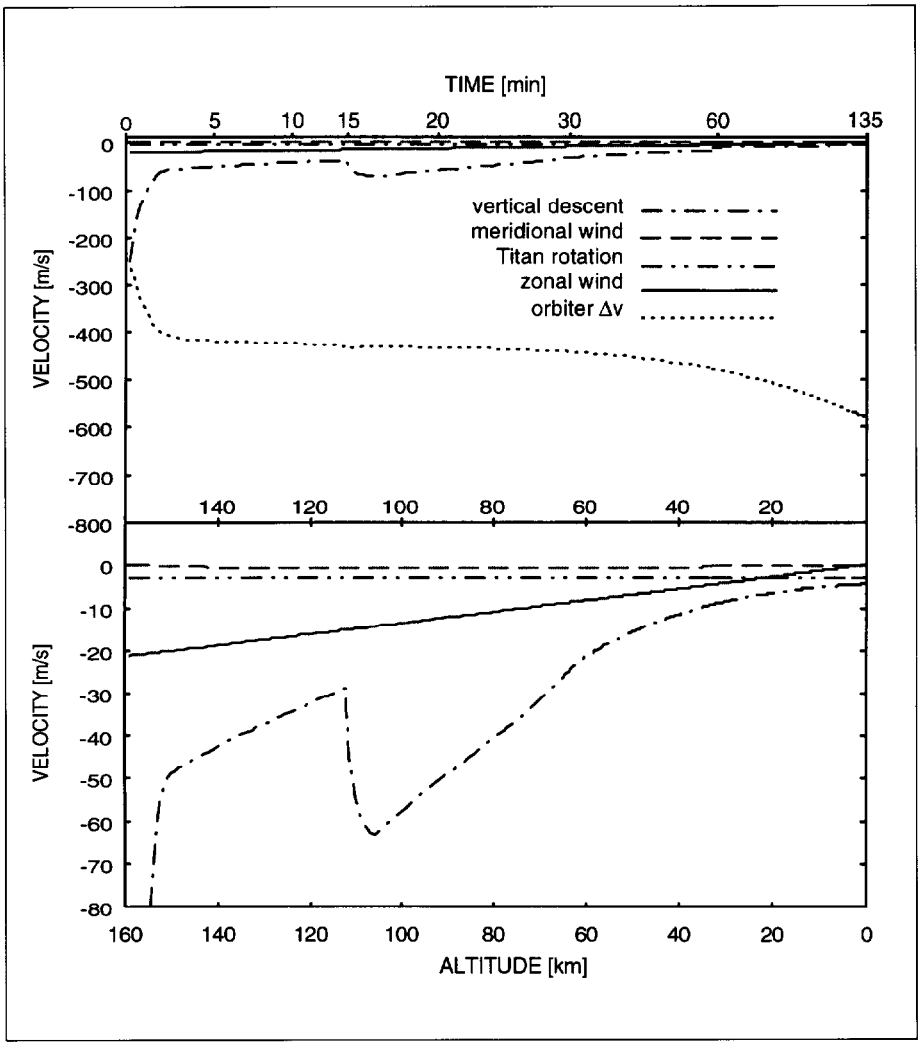

Fig. 4. Velocity contributions to PRL Doppler shift for the nominal Huygens descent profile.

of the spin rate error (1σ) of $\delta\omega = \pm 0.27/(\omega\tau)^{1/2}$ rpm, where ω is the spin rate in rpm and τ is the integration time in minutes. For a representative value of $\tau = 1$ min, this yields a relative error of 27% just before impact, when the Probe spin rate is expected to be ~1 rpm. The relative error is much smaller at higher altitudes where the spin rate is greater (e.g. ~0.9% for $\omega = 10$ rpm, $\tau = 1$ min). An improvement in this estimate from the Doppler data can be achieved by including the signal level data. As the radiation pattern of the Probe Transmitter Antenna (PTA) is asymmetric, the Probe's rotation phase can be determined from the phase of the received signal level modulation. The amplitude of the PTA's cyclic variation will be ~ ±2 dB during each rotation.

3.2.2 Vertical resolution: Probe response time

It is important to characterise the wind shear and turbulence in Titan's atmosphere with DWE measurements of the smaller-scale Probe motion due to wind gusts (Strobel & Sicardy, 1997). To a good approximation (Atkinson, 1989), the Probe response to a horizontal wind gust of magnitude u_0, applied at time $t = 0$, is given by:

$$\dot{x}(t) = u_0 \left[1 - \exp\left(-\frac{g}{V_T} t \right) \right] \tag{18}$$

where V_T is the terminal velocity determined from the force balance (7) between

gravity and the drag force (for $\dot{z} = 0$) given by

$$V_T \approx \sqrt{\frac{2mg}{C_D A \rho}} \tag{19}$$

Referring to (18), the Probe evidently adjusts itself to the wind on time scales of the order of:

$$\tau = \frac{V_T}{g} \tag{20}$$

The relaxation time constant τ at some level in the atmosphere is equal to the ratio of the Probe terminal velocity V_T to the acceleration of gravity g *at that level*. Both the descent velocity (19) and the Probe response time (20) vary with atmospheric density as $\rho^{-1/2}$.

If the Probe suddenly encounters a wind gust, the Probe horizontal velocity will adjust itself to a factor $(1 - e^{-1})$, or about 63% of the gust velocity, in a time equal to the time constant (20). In this time, the Probe has descended through a distance

$$l_{min} = V_T \tau = \frac{V_T^2}{g} \tag{21}$$

Wind shears contained within a spatial layer smaller than l_{min} will have essentially no effect on the Probe. The spatial scale l_{min} thus represents the minimum (vertical) size of atmospheric structure detectable by monitoring the PRL Doppler profile. Invoking (19) and (20), it is seen that l_{min} is inversely proportional to the atmospheric density and independent of g:

$$l_{min} = \frac{2C_B}{\rho} \tag{22}$$

Using the Titan atmospheric pressures and densities from Lellouch et al. (1989), the Probe descent velocity V_T, response time τ and minimum scale sizes l_{min} are tabulated in Table 1, based on the nominal descent profile of duration 135 min. Under the initially large parachute ($C_B \simeq 8$ kg/m^2) in the upper atmosphere (above ~115 km), the Probe motion will reflect atmospheric structure with kilometre size scales. Near the surface, where $C_B > 50$ kg/m^2 and V_T is much smaller, the minimum detectable structure size is of the order of 20 m.

3.3 Doppler wind recovery algorithm

A robust zonal wind recovery algorithm for the Cassini-Huygens scenario has been developed by Atkinson et al. (1990). Much of the formalism has been carried over from

Table 1. Probe descent velocity, response time and vertical resolution.

time (min)	*altitude* (km)	*P* (mbar)	ρ (kg/m^3)	C_B (kg/m^2)	V_T (m/s)	τ (s)	l_{min} (m)
8	130	4	0.009	8	47.0	38.6	1815
40	50	77	0.363	52	19.3	14.8	286
82	20	487	2.19	53	8.0	6.0	48
105	10	859	3.58	53	6.3	4.7	30
120	5	1120	4.43	53	5.7	4.2	24
135	0	1440	5.38	56	5.3	3.9	21

the experience gained from a very similar DWE investigation on Galileo (Pollack et al., 1992). An essential prerequisite to application of the algorithm is an accurate reconstruction of the Probe-Orbiter relative geometry. It is *initially* assumed that the Probe's position is not affected by the integrated effect of the winds. Once a preliminary wind profile is calculated, the Probe descent position can be updated to reflect the integrated effect of the winds on the Probe descent longitude, and the wind profile is recalculated with the new time-varying Probe longitudes. An important assumption is that the zonal winds are dominant, with the possible exception of the last few kilometres above the surface.

The zonal wind profile derived from the DWE measurements on Galileo is a *relative* (wind shear), rather than *absolute*, profile. This is because of the rather large uncertainty in the actually transmitted frequency from the quartz USO on the Galileo Probe. The 'constant' of the integration, i.e. a value of the wind u_N at a specific time t_N, must be determined by independent means. This problem does not exist with the Huygens DWE because the absolute fractional frequency uncertainties inherent to the TUSO and RUSO are of the order $\delta f/f \simeq 2 \times 10^{-10}$.

Under these circumstances, the accuracy with which the zonal winds can be recovered is determined by the imperfect knowledge of the Probe/Orbiter trajectory. Of lesser importance are second-order Taylor, Doppler and Special Relativistic terms that are usually dropped in order to keep the recovery problem linear, and environmental effects due to S-band signal propagation through a refracting, attenuating atmosphere (e.g. Bird, 1997). Trajectory and oscillator drift errors introduce a small time-varying component into the Probe-Orbiter relative velocity that cannot be distinguished from atmospheric winds. A detailed treatment of the effects of these various errors for the recovery of the zonal wind height profile may be found in Atkinson et al. (1990).

In order to better understand the limitations of the recovery algorithm, we numerically simulated the wind recoveries for a variety of different trajectories, wind environments and errors. Here we summarise the results from several of those simulations and compare the recovered wind profile to the ideal case, where no frequency errors, trajectory uncertainties or anomalous wind regions exist. In all cases the input wind profile is a 'Flasar-type' model, a linearly increasing zonal wind with height, the direction and magnitude of which are variable parameters of the simulation. Wind recovery results for four different models are shown in Fig. 5 after five iterations.

The input errors used in the simulations of Fig. 5 were representative for the Huygens descent on Titan. The largest error sources are those due to Probe entry longitude (0.7°), Probe entry latitude (0.1°), Probe descent velocity ($0.005\dot{z}$) and the maximum possible USO frequency drift (0.4 Hz in 2.5 h). In spite of the non-negligible trajectory and frequency errors, the recovered wind profiles in Fig. 5 are very good facsimilies of the input profiles. Differences are apparent only in the upper levels of the atmosphere on the scale of the graph. The errors decrease during the Probe descent — in these simulations constrained to be zero at Titan's surface.

The touchdown longitude ϕ_{td} is located about 6° (260 km) east of the entry longitude for the case with the nominal prograde wind profile. The Probe's mean speed in its easterly drift is $\simeq$100 km/h (28 m/s). Since the drift speed can be higher than the vertical descent velocity, the flight path to the surface can become rather flat. As expected from (7), the vertical descent time is only weakly dependent on the zonal wind u.

The quality of the wind recovery for the four examples of Fig. 5 is summarised in Table 2, which shows (a) the mean error in the determination of the zonal wind over the height interval 0-100 km (δu in m/s), and (b) the error in the determination of the impact longtude ($\delta\phi_{td}$ in degrees).

Table 2. Mean zonal wind and impact longitude errors.

Input wind model	δu (m/s)	$\delta\phi_{td}$ (°)
1 × prograde	1.14	0.48
2 × prograde	2.34	0.22
1 × retrograde	-2.57	1.23
2 × retrograde	-6.42	1.96

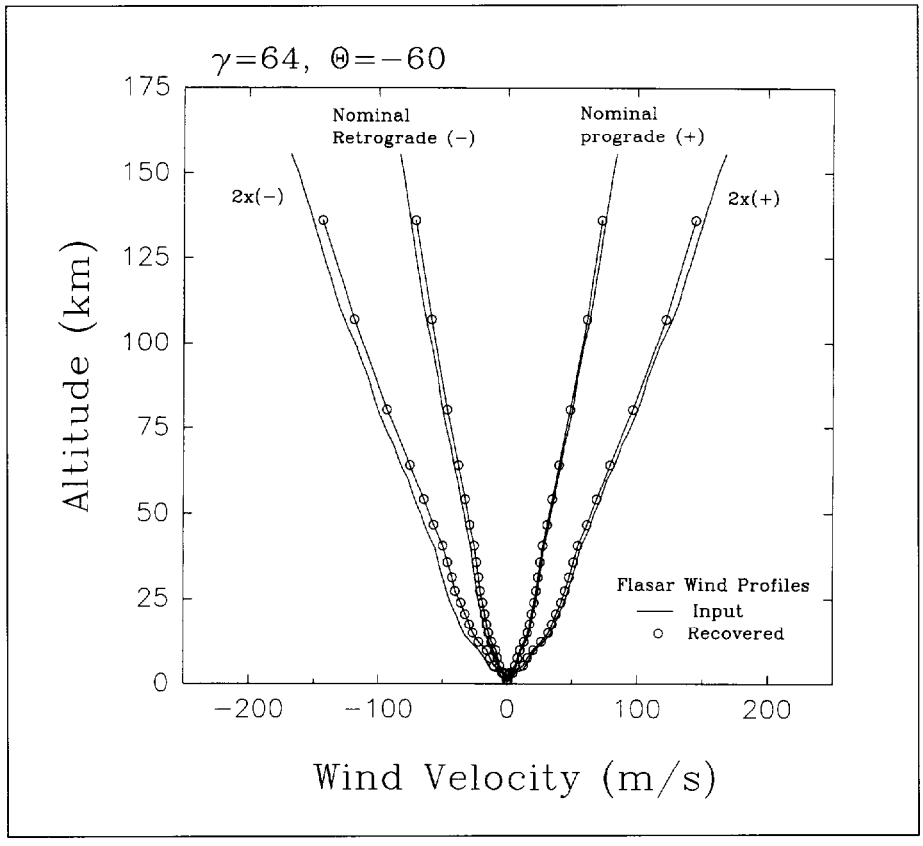

Fig. 5. Height profiles of input and recovered zonal wind velocities.

Additional simulations verified that the wind recovery algorithm is not affected by an input wind profile with a region of high shear, i.e. the wind recovery is not limited to smooth and slowly varying horizontal winds. As noted in the previous section, however, the detectability of fine wind structure is limited by the Probe response time (20).

3.4 End-to-end measurement concept

DWE is the only Huygens investigation with 'science hardware' on both the Probe and within the Probe Support Avionics (PSA) of the Probe Support Equipment (PSE) on the Orbiter. An end-to-end block diagram of the DWE experimental configuration is shown in Fig. 6.

The DWE-TUSO on the Huygens Probe is the primary signal generator used to drive the PRL of Transmitter A (Tx A). In case of failure, the driver signal can be switched to an internal temperature-controlled quartz oscillator (TCXO) with a frequency stability approximately 1000 times worse than the TUSO. The choice of oscillators for Tx A will be made before Probe-Orbiter separation, based on the performance of the TUSO and TCXO during the regular cruise phase checkouts.

The 10 MHz output of the TUSO is upconverted to the PRL frequency of 2040 MHz, at which point it is transmitted via one of two routes to PSA Receiver A (Rx A) on the Orbiter. During cruise checkouts the signal is attenuated and sent via the radio frequency built-in-test equipment (RF-BITE) across the Umbilical Separation Mechanism (USM). During the Titan descent the signal is amplified for free-space RF transmission via the PTA to the Cassini HGA. The centre frequency of PSA Rx A is tuned to the nominal Tx A output frequency at 2040 MHz in checkout mode and is shifted by +38.5 kHz for descent mode.

All timing and signal generator requirements for Rx A are controlled by the DWE-RUSO, which is virtually identical to the TUSO on the Probe. Similar to the Probe

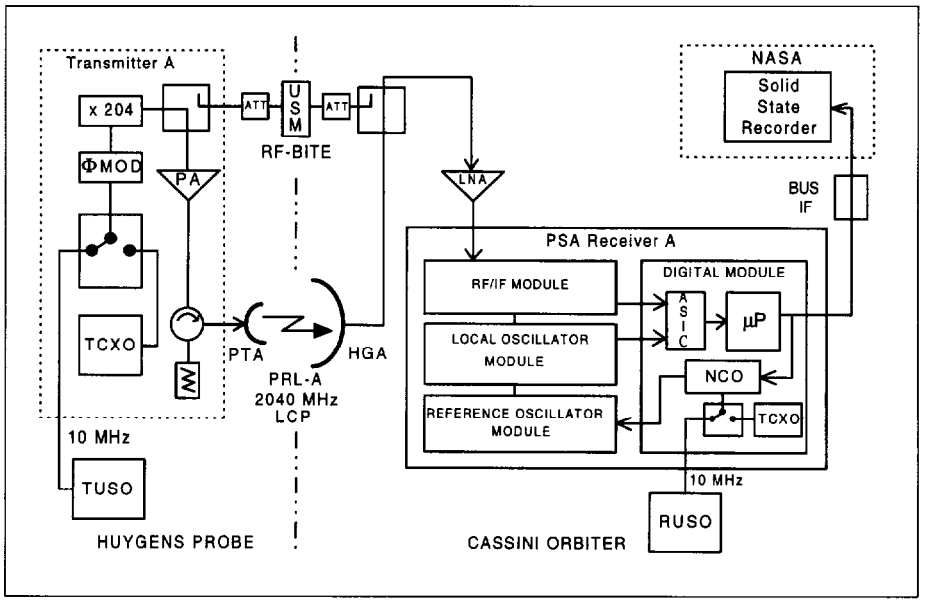

Fig. 6. End-to-end configuration of the Doppler Wind Experiment.

side, switching to a back-up TCXO is possible in case the RUSO fails. After downconversion, the PSA receiver phase locks onto the PRL signal, the loop control being governed by a numerically controlled oscillator (NCO). The digitised values of the changes in NCO frequency required to maintain phase lock, an 'NCO control word' of 20 bits, is written to the PSE housekeeping (HK) data at 8 samples/s. The PRL signal level is monitored at the same sample rate by recording the PSA receiver automatic gain control (AGC; length 16 bits). The frequency resolution due to the data digitisation is governed by the internal PSA receiver clock and is given as ~60 MHz, which is very close to the least significant bit written into the NCO control word (48 MHz). The range of Doppler shifts accomodated by the 20-bit NCO control word is ±12.69 kHz (±1866 m/s). The NCO control word and AGC data are routed to the solid state recorders on the NASA side of the Orbiter for later playback to Earth. The 'redundant' data from PSA receiver B (Rx B) are generated and received using standard TCXOs and thus not expected to yield information about the Probe's drift motions. Nevertheless, these data will also be recorded for the AGC information, thereby providing a control value for comparison with the data from Rx A.

The only DWE data transmitted with the PRL telemetry are three temperature measurements (8 bits each) and one bi-level lock status bit, which are recorded every 16 s as part of the Probe housekeeping (HK) telemetry blocks. The associated DWE 'bit rate' of these HK data is thus only ~1.6 bit/s. Analogous HK-data are recorded at 25 bit/s on the PSE side from the RUSO. The quantities comprising DWE science data, the NCO control word for the frequency and the AGC for the signal level of the PRL are recorded at 288 bit/s. Assuming these data are recorded for the longest possible Huygens mission of 3 h (including 30 min on the surface), the total amount of cumulated DWE data for one chain will be ~425 kbyte. The Tx/Rx chain B, to be analysed primarily for its AGC information (no RUSO data), will generate another ~391 kbyte. Noting that these data will be stored redundantly for later playback to Earth, we arrive at a grand total for the DWE data volume of 1.632 Mbyte.

The TUSO will be powered up before Titan atmospheric entry at the time t_0 − 17 min 46 s, in order that it be given sufficient warm-up time to achieve the required frequency stability. The RUSO, which will be turned on at t_0 − 30 min, is less critical because of its comparitively safe location onboard the Orbiter. The DWE-USO frequency stability will be monitored during the regularly scheduled Probe cruise checkouts en route to Saturn. The last such rehearsal will occur during the initial Saturn orbit, about 10 days before Probe separation.

4. DWE Instrumentation: Ultrastable Oscillator (USO)

4.1 Transmitter and receiver USO programmes

Two ultrastable oscillators, a TUSO for the transmitter on Huygens and a RUSO for the receiver on Cassini, have been constructed as identical units within one and the same USO programme in order to minimise costs. The contractor for this work is Daimler-Benz Aerospace (DASA), Satellite Systems Division, in Ottobrunn, Germany. The DASA design concept is based on a space-qualified rubidium oscillator Physics Package supplied by Ball Efratom Elektronik GmbH. The TUSO/RUSO combination represents the first use of rubidium oscillators on a deep space planetary mission.

A total of six USO models have been built. The single Structural, Thermal and Pyrotechnic Model (STPM) was delivered for system testing on schedule in April 1994. The two Electrical Models (EM), one TUSO and one RUSO, were delivered in November 1994 to the System AIV (Assembly, Integration and Verification) Program at DASA. Three interchangable units of flight standard (FM) have been fabricated: one TUSO FM, one RUSO FM and one Qualification Flight Spare (QFS, a refurbished unit used for qualification testing at unit level).

4.2 USO mechanical/electrical characteristics

The DWE USOs are designed to withstand the Cassini/Huygens launch and cruise phase (10 years in the event of a 1999 backup launch), as well as the Huygens atmospheric entry and descent on Titan. The TUSO on Huygens is exposed to higher mechanical loads than the RUSO on Cassini. The most critical factor for the TUSO, a major driver in the selection of an ultrastable oscillator based on rubidium technology, is the peak deceleration of up to 16.1 g during the Huygens entry phase. It could not be guaranteed that the required frequency stability of $\delta f_0/f_0 < 2 \times 10^{-10}$ (f_0 = nominal output frequency) could be met after the Probe entry into Titan's atmosphere with a state-of-the-art quartz oscillator. The high mechanical load during entry might cause a deformation of the internal quartz fastening system in combination with an unpredictable frequency offset and an unknown frequency relaxation time. A similar problem with continuously varying mechanical stresses on the quartz box was foreseen in the subsequent pressure variation from 0 bar to 1.5 bar during descent. These adverse effects can be averted with a rubidium oscillator, for which the frequency source is also a quartz, because the nominal output frequency is locked to the very stable frequency of the rubidium ground-state hyperfine transition.

The basic principle of a rubidium oscillator (see Fig. 7) is to employ the two ground-state hyperfine levels A and B and a much higher optical level C of rubidium atoms to produce an error signal for the control circuit of a voltage-controlled quartz oscillator VCXO. IR light from a rubidium lamp is filtered and passes through the heated rubidium resonance cell with a frequency $\nu_{CA} = \nu_C - \nu_A$, exciting transitions to state C of the rubidium gas. Atoms in level C drop back after a very short time either to state A or, with less probability, to state B. As atoms in state A are continuously re-excited to C, the population of level B steadily increases ('optical pumping'). When state A is depopulated, a maximum photocurrent is produced in the photocell as the light is no longer attenuated by excitation processes from level A to C. The HF-signal of the synthesiser, which is upconverted from the quartz output signal, also irradiates the rubidium resonance cell. The synthesiser is calibrated to generate the exact resonance frequency $\nu_{BA} = \nu_B - \nu_A \approx 6.835$ GHz if the quartz has its nominal output frequency. At this frequency, atoms in level B de-excite to state A, thereby inducing a minimum photocurrent, because the rubidium vapour is no longer transparent to the frequency ν_{CA}. Deviations from the minimum current condition are produced by deviations in the nominal VCXO output frequency. The current dip, however, is very small (0.1% of the total photocurrent) and not suitable for a DC detection. To circumvent this shortcoming, the synthesiser frequency is modulated at an audio

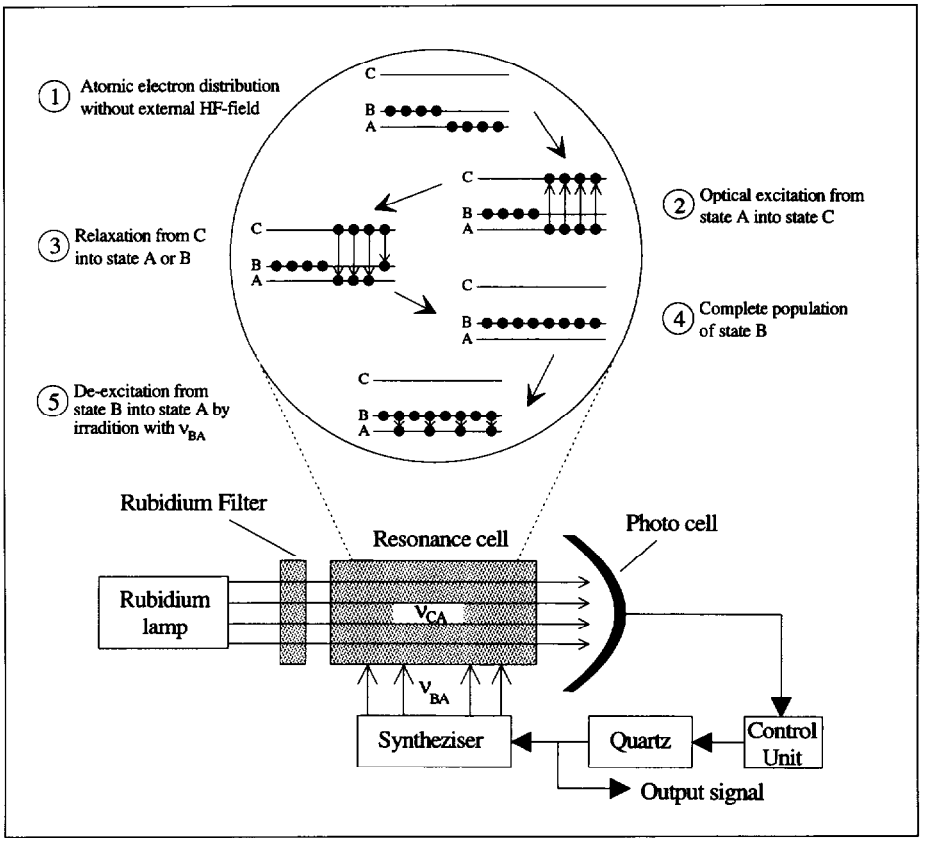

Fig. 7. Operation principle of a rubidium oscillator.

frequency ν_m = 127 Hz. The similarly modulated photocurrent can now be AC-detected by synchronous current demodulation. There is a positive correlation between the sign of the current error signal (positive or negative) and the offset from the nominal quartz output frequency. This error signal is used to lock the nominal quartz signal to the rubidium resonance frequency by varying the quartz control voltage.

The USO consists of the Physics Package (rubidium resonance cell and lamp) and several printed circuit boards, which contain discrete electronic elements as well as integrated circuits. The USO electronics and the Physics Package are integrated into an aluminium box, which is constructed as a Faraday cage to avoid electromagnetic contamination of the USO environment. The USO box is attached to the experiment platform via four mounting studs, thereby providing a thin air buffer for better insulation from the mounting platform. This reduces the USO conductive heat loss, saving power that would otherwise be needed for heating.

The box surface is plated with nickel and coated with Chemglaze Z 306. The total mass of the USO is ~1.9 kg. The electronics and Physics Package is surrounded by μ-metal shielding to minimise the effects of changes in the external magnetic fields that range from $>10^4$ nT on Earth to essentially zero at Titan. Variations in the ambient magnetic field induce a change in the Rb hyperfine resonance frequency and thus a frequency shift in the USO output signal. Radiation-sensitive USO components such as transistors and analogue ICs are radiation-hardened up to 10 krad. While the maximum radiation dose for the Probe TUSO is ~5 krad, the RUSO on the Orbiter will be exposed to about 18 krad in the event of a 1999 launch. In order to provide additional radiation protection for the RUSO, the critical components of both USO units are shielded with tantalum caps (thickness ~1 mm). Radiation shielding contributes about 10% to the total USO mass budget.

A block diagram of the USO unit is shown in Fig. 8. The external supply voltage of 28 V (TUSO) or 30 V (RUSO), is transformed down to 5 V and 17 V by the

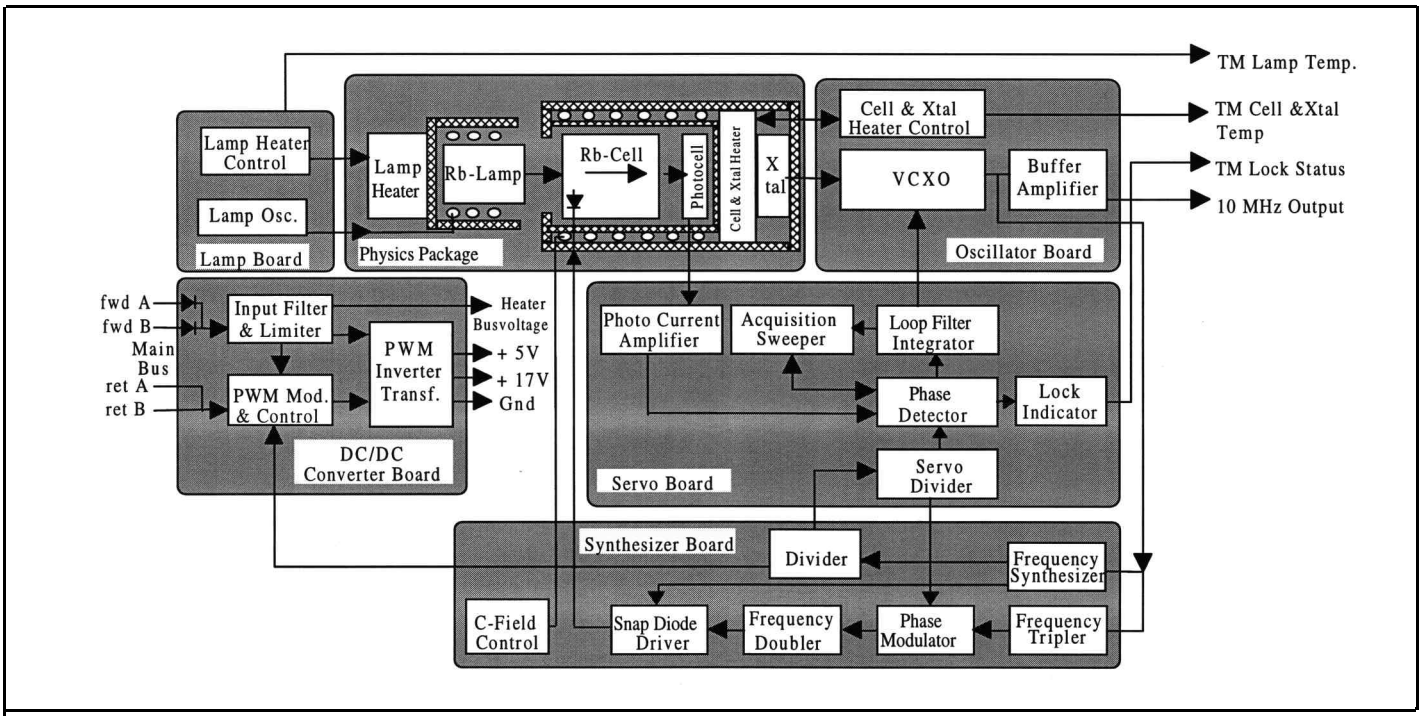

Fig. 8. USO block diagram.

DC/DC converter. The converter control signal is provided by the synthesiser, synchronised to the quartz output signal. The VCXO quartz, located on the Oscillator Board, provides the 10 MHz output through a buffer amplifier. The same signal is upconverted by the synthesiser to the rubidium resonance frequency. The photocurrent of the Physics Package is routed to the Servo Board, which generates the error signal for the voltage control of the VCXO. The heater control of the rubidium lamp within the Physics Package is located on a separate Lamp Board. Three analogue sensors monitor the temperatures of the rubidium lamp, rubidium cell and VCXO, respectively. A bi-level lock indicator flips from '0' to '1' whenever the quartz output signal is in lock with the rubidium resonance frequency. The temperatures and lock indicator signal are part of the Huygens HK data. Table 3 summarises the USO mechanical and electrical characteristics.

4.3 USO frequency characteristics

The USO long-term frequency stability requirement of $\delta f_0/f_0 \leq 2 \times 10^{-10}$ is critical for a successful Doppler Wind Experiment. By 'long-term', it is meant that the uncertainty in the frequency must be constrained within these limits for the maximum expected duration of the atmospheric descent (2.5 h), i.e. the total frequency shift of the PRL signal is <0.4 Hz over the entire Huygens mission. Assuming a typical DWC angle of 65°, an unwanted frequency shift of this magnitude would be indistinguishable from

Table 3. USO mechanical and electrical characteristics.

Mass	1.90 ± 0.15 kg
Dimensions (length × width × height)	180 × 149 × 118 mm
Warm-up Power	P_{wu} = 18.2 W (≤ 30 min)
Steady State Power at baseplate temperature T	P_{ss} = 10.375 - 0.0625T (W)
Output Frequency	10 MHz ± 0.1 Hz
Output Signal Level	0 ± 1 dBm into 50 Ω
Warm-up Time to $\delta f_0/f_0 = 2 \times 10^{-10}$	≤30 min
Supply Voltage (TUSO)	$28^{+0.35}_{-0.63}$ V
Supply Voltage (RUSO)	$30^{+1.5}_{-3.38}$V

Table 4. Fractional change of USO output frequency.

Environmental factor	*fractional frequency change* $\delta f_0/f_0$	*worst case: Huygens descent* *TUSO*	*RUSO*
Temperature (per °C)	3×10^{-12}	$\Delta T\approx 15$°C	$\Delta T\approx 5$°C
Pressure P (per bar)	1×10^{-12}	$\Delta P\approx 1.6$ bar	$\Delta P\approx 0$ bar
Acceleration A (per g)	4×10^{-12}	$\Delta A\approx \pm 1.0\ g$	$\Delta A\approx \pm 0.1\ g$
Magnetic field B (per G)	2×10^{-12}	$\Delta B\approx 1$ mG	$\Delta B\approx 0.1$ mG

a zonal wind with velocity of ~0.15 m/s. This USO frequency stability is thus mandatory for achieving the primary DWE goal, a determination of Titan's zonal wind height profile with an accuracy well below the ±1 m/s level. This must be maintained throughout the entire Huygens mission, in spite of many rather severe changes in the environmental conditions (temperature T, pressure P, acceleration A and magnetic field B). Generally, this requirement can be expressed by:

$$\left|\frac{\delta f_0}{f_0}\right| = \frac{1}{f_0}\sqrt{\left(\frac{\delta f_0}{\delta T}\Delta T\right)^2+\left(\frac{\delta f_0}{\delta P}\Delta P\right)^2+\left(\frac{\delta f_0}{\delta A}\Delta A\right)^2+\left(\frac{\delta f_0}{\delta B}\Delta B\right)^2+\left(\frac{\delta f_0}{\delta X}\Delta X\right)^2} \leq 2\times10^{-10} \tag{23}$$

where 'X' collectively labels other factors, e.g. the variation of the USO supply voltage. Typical values for the expected fractional change in the USO output frequency are listed in Table 4.

Although not as critical as the long-term frequency stability, the short-term frequency stability is another criterion for the frequency quality of the USO. The short-term frequency stability is characterised by the mean fractional frequency deviation

$$\sigma = \frac{\Delta f_0}{f_0} \tag{24}$$

This quantity, sometimes called the 'Allan deviation', depends on the integration time τ (see also equation 26). The specified USO short-term frequency stabilities are shown in Table 5. These values are sufficient to detect PRL frequency modulations owing to atmospheric turbulence as well as the Probe's pendulum and rotational motion. Table 6 lists the specifications on the phase noise of the output signal spectrum for various displacements from the centre peak.

Table 5. USO short-term frequency stability.

Integration time τ (s)	$\Delta f_0/f_0$
0.1	6×10^{-11}
1	1×10^{-11}
10	5×10^{-12}
100	1×10^{-12}

Table 6. USO phase noise.

Displacement (Hz)	*Phase noise (dBc)*
1	-90
10	-120
100	-140
1000	-150

4.4 USO test programme

At this writing, only results from the EM test programme are available. The DWE USO Electrical Model is shown in Fig. 9, before integration, with the aluminum housing removed.

A USO test assembly (block diagram: Fig. 10), developed at the University of Bochum, is used at the unit level to determine USO frequency characteristics. Of particular interest is the frequency stability of the USO on all time scales. It is also necessary to characterise the repeatability of the long-term drift of the USO in order to correct for this effect under the conditions of the Huygens descent.

The frequency measurement procedure is based on a comparison of the test frequency f (DWE-USO) with a reference signal f_0 (rubidium reference oscillator), the frequency stability of which is better than or equal to that of the test signal. Using a synthesiser, the reference frequency is offset from the nominal frequency of the test object f_0 by a known amount f_{offset}. The frequency difference of the two signals is

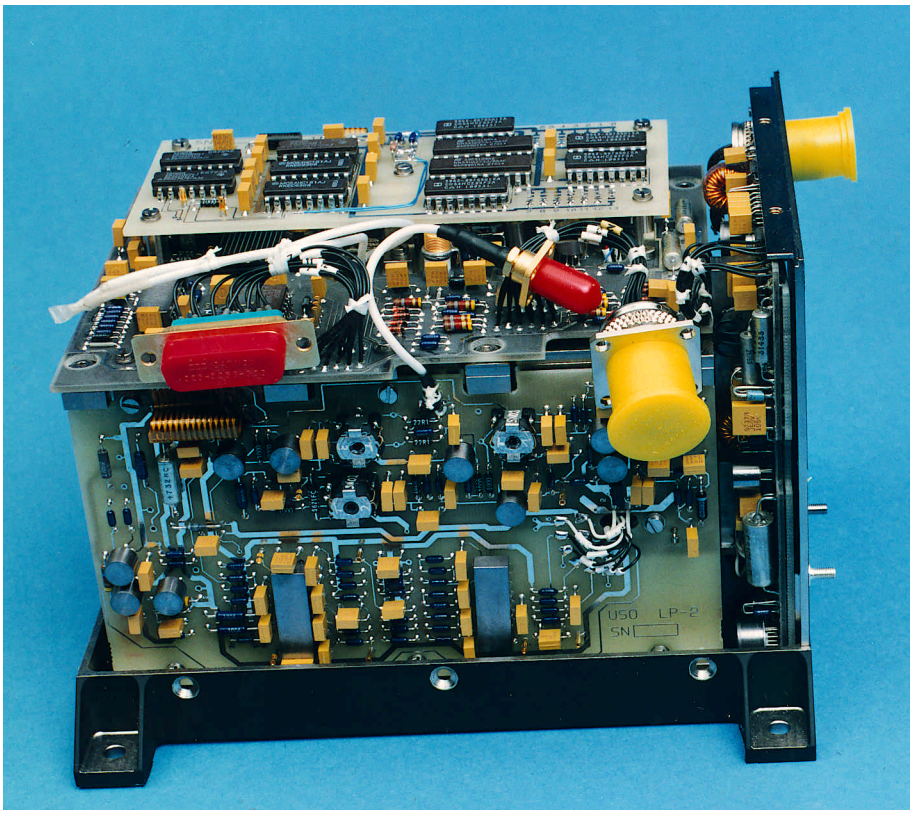

Fig. 9 The DWE-TUSO engineering model. The input power connector and grounding studs are on the right side. The remaining ports facing out of the page are (from left) test connector (red, elongated), the 10 MHz RF output (red, round) and the telemetry output connector (yellow).

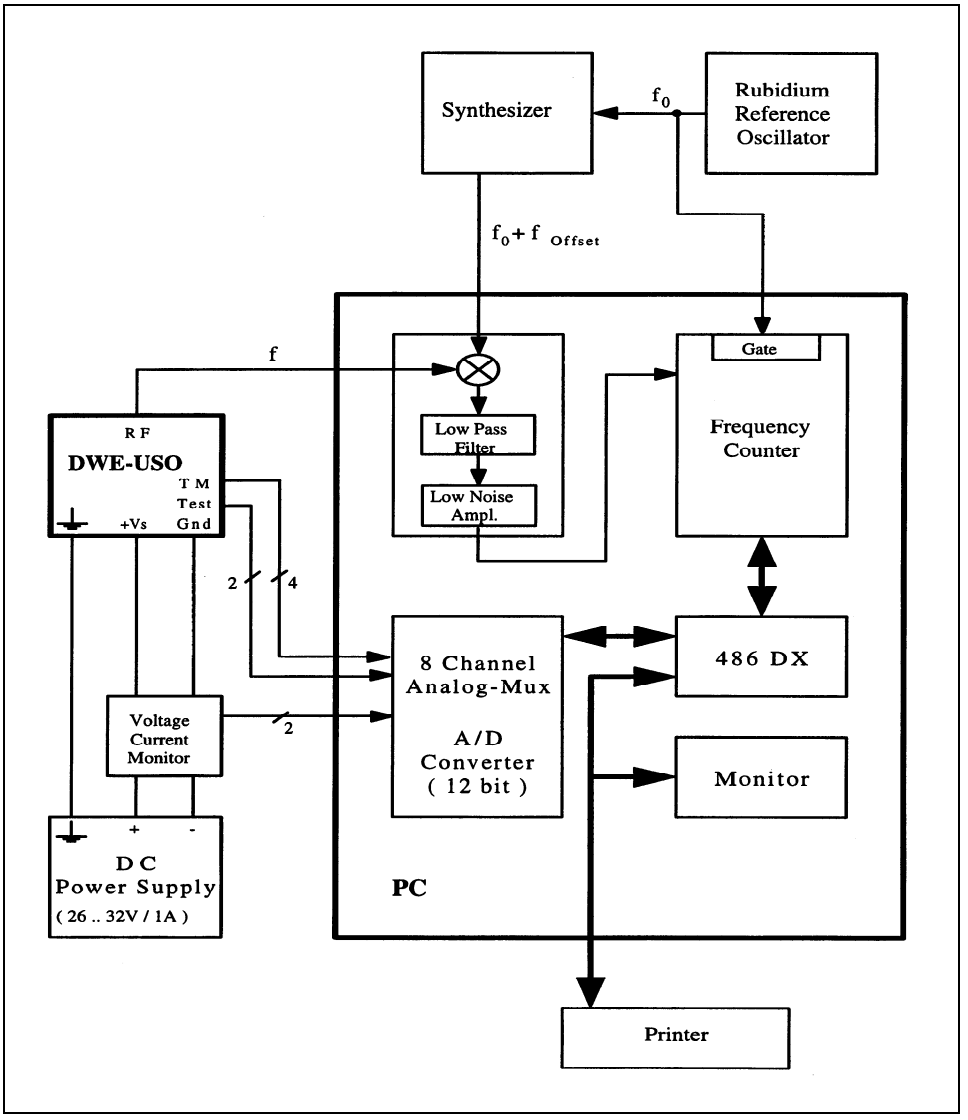

Fig. 10. Block diagram of the USO test assembly.

generated with the help of a mixer and then measured by a frequency counter. Following a fully automated procedure, both the long-term and short-term stabilities of the test object are determined by recording the frequency difference for an appropriately long interval (nominal test run: 3 h). The reference and offset frequencies, as well as the integration and sample times can be adjusted as necessary with respect to their default values for each individual run.

The number of single measurements is defined by the ratio of the adjusted total measurement time to the mean duration of the single measurement cycle. A single measurement cycle consists of the adjusted fixed integration time and the counter register read-out time. The read-out phase requires about 20 ms. The mean duration of one measurement cycle is thus about 1.02 s for an integration time of τ = 1 s, and 10.02 s for τ = 10 s, respectively. The absolute frequency $f(t)$ and the Allan variance σ^2 are then derived as follows:

$$f(t) = \Delta f + f_0 - f_{\text{offset}} \tag{25}$$

$$\sigma^2(\tau) = \frac{1}{N} \sum_{k=1}^{N} \frac{(\bar{y}_{k+1} - \bar{y}_k)^2}{2} \tag{26}$$

where $\bar{y}_k = \Delta f_k/f_0$, $\Delta f_k = m_k/\tau$, and m_k is the k^{th} cycle count over the integration time τ.

Examples of short-term stability results from a typical test run during the unit-level TUSO-EM programme are displayed in Fig. 11. Running measurements of σ, defined by (26) are made for integration times τ = 1 s & 10 s. Each point in Fig. 11 represents 100 such measurements. The mean values of the Allan deviation in this case were $<\sigma(1\text{ s})> = 1.8\times10^{-11}$ and $<\sigma(10\text{ s})> = 5.5\times10^{-12}$, respectively.

The behaviour of the USO output frequency as a function of time from switch-on is shown in Fig. 12 for two test models, one with and one without a temperature-compensating magnetic control loop. These tests were performed at an ambient temperature of +25°C.

After reaching its asymptotic value, the output frequency of both models stays within a band $\delta f/f < \pm 2\times10^{-10}$. The model without magnetic compensation was found to require too much time to warm up and also exhibited undesireable variations in

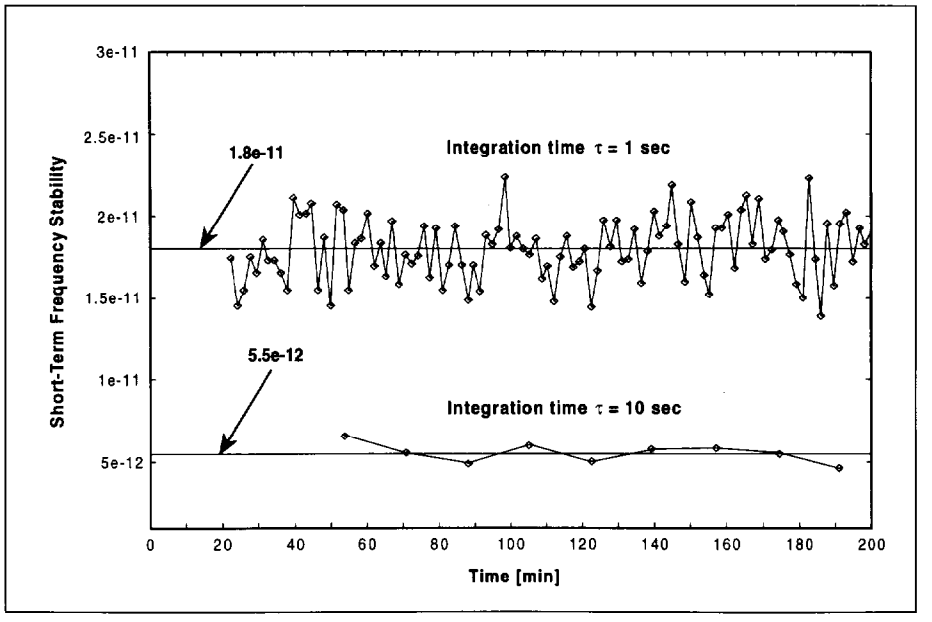

Fig. 11. Short-term frequency stability $\Delta f_0/f_0$ of the DWE-TUSO Electrical Model.

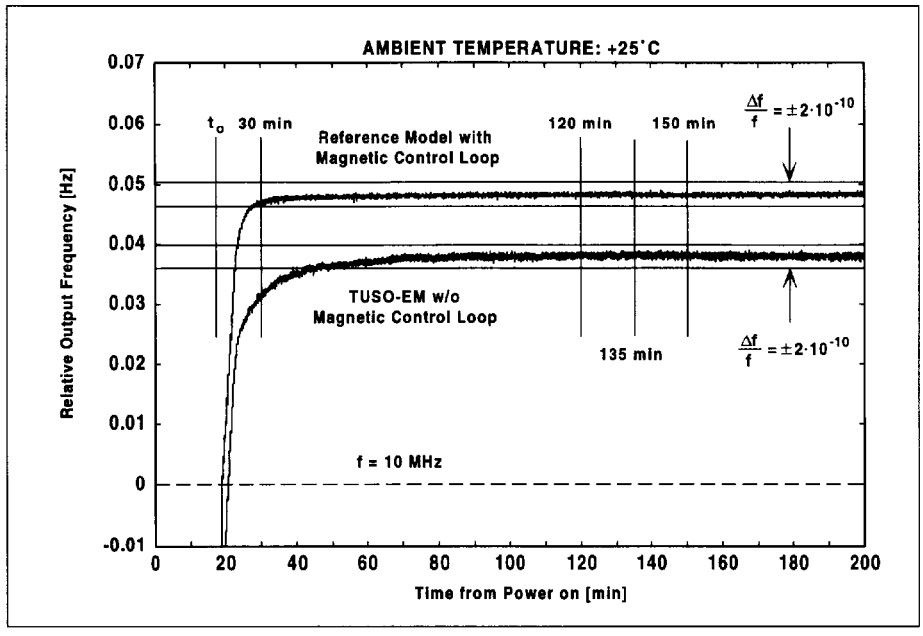

Fig. 12. USO output frequency as a function of time from switch-on.

asymptotic output frequency with temperature. Significant improvement was achieved by implementation of a magnetic control loop, which exploits the sensitivity of the rubidium hyperfine transition to the strength of the magnetic field in the rubidium cell. The strength of the magnetic field applied to compensate for the thermal drift is determined via a feedback loop using the thermal sensor in the crystal oscillator. Preliminary results from recent thermal vacuum tests (FM Test Program) over an ambient temperature range from −30°C to +60°C indicate that: (a) the USO warm-up time is always <30 min, and (b) the variation in mean asymptotic frequency is $<2 \times 10^{-9}$.

5. Conclusions

The Huygens Doppler Wind Experiment is designed to determine the velocity of Titan's zonal winds. The wind is measured over a height range of 0-160 km from its Doppler signature on the Probe's radio relay signal to the Orbiter. The stringent frequency stability required for the DWE measurement is assured by (a) generating the transmitted signal with an externally-supplied ultrastable oscillator (TUSO), and (b) providing the receiver with an identical ultrastable external oscillator (RUSO). Information on Probe dynamics (spin rate, spin phase, parachute swing) and large-scale turbulence in Titan's atmosphere are secondary objectives of the investigation. The reconstructed Probe trajectory using DWE data provides the best estimate of Huygens' final place of rest on Titan.

Acknowledgements

This paper presents results of a research project partially funded by the Deutsche Agentur für Raumfahrtangelegenheiten (DARA) GmbH under contract 50 OH 9207. The responsibility for the contents is assumed by the authors.

References

Allison, M. (1992). A preliminary assessment of the Titan planetary boundary layer. In *Symposium on Titan*, ESA SP-338, ppl13-118.

Allison, M., Del Genio, A. D. & Zhou, W. (1994). Zero potential vorticity envelopes for the zonal-mean velocity of the Venus/Titan atmospheres. *J. Atmos. Sci.* **51**, 694-702.

Atkinson, D. H. (1989). Measurement of planetary wind fields by Doppler monitoring of an atmospheric entry vehicle. Ph.D. Thesis, Washington State University, Pullman WA, USA, 609pp.

Atkinson, D. H., Pollack, J. B. & Seiff, A. (1990). Measurement of a zonal wind profile on Titan by Doppler tracking of the Cassini entry probe. *Radio Sci.* **25**, 865-882.

Bird, M. K. (1997). Atmospheric attenuation of the Huygens S-Band Radio Signal during the Titan Descent. In *Huygens: Science, Payload and Mission*, ESA SP-1177 (this volume).

Caldwell, J., Wu, N., Smith, P. H., Lorenz, R. D. & Lemmon, M. T. (1996). Hubble Space Telescope Imaging of Titan in 1995. *Bull. Am. Astron. Soc.*, **28**, 1132.

Coustenis, A. (1990). Spatial variations of temperature and composition in Titan's atmosphere: Recent results. *Ann. Geophysicae* **8**, 645-652.

Del Genio, A. D., Zhou, W. & Eichler, T. P. (1993). Equatorial superrotation in a slowly rotating GCM: Implications for Titan and Venus. *Icarus* **101**, 1-17.

Flasar, F. M., Allison, M. & Lunine, J. I. (1997). Huygens Probe wind drift: science issues and recommendations. In *Huygens: Science, Payload and Mission*, ESA SP-1177 (this volume).

Flasar, F. M. & Conrath, B. J. (1990). Titan's stratospheric temperatures: A case for dynamical inertia? *Icarus* **85**, 346-354.

Flasar, F. M., Samuelson, R. E. & Conrath, B. J. (1981). Titan's atmosphere: temperature and dynamics. *Nature* **292**, 693-698.

Flury, W. (1986). Cassini Mission - Titan Probe trajectory. In *The Solid Bodies of the Outer Solar System*, ESA SP-242, pp237-281.

Hanel, R. et al. (1981). Infrared observations of the Saturnian system from Voyager 1. *Science* **212**, 192-200.

Hinson, D. P. & Tyler, G. L. (1983). Internal gravity waves in Titan's atmosphere observed by Voyager radio occultation. *Icarus* **54**, 337-352.

Hourdin, F., Talagrand, O., Sadourny, R., Courtin, R., Gautier, D. & McKay, C. P. (1995). Numerical simulation of the general circulation of the atmosphere of Titan. *Icarus*, **117**, 358-370.

Hubbard, W. B. et al. (1993). The occultation of 28 Sgr by Titan. *Astron. Astrophys.* **269**, 541-563.

Lebreton, J.-P. & Matson, D. L. (1997). The Huygens Probe: Science, Payload and Mission Overview. In *Huygens: Science, Payload and Mission*, ESA SP-1177 (this volume).

Lellouch, E., Coustenis, A., Gautier, D., Raulin, F., Dubouloz, N. & Frère, C. (1989). Titan's atmosphere and hypothesized ocean: a reanalysis of the Voyager 1 radio-occultation and IRIS 7.7 μm data. *Icarus* **79**, 328-349.

Lindal, G. F., Wood, G. E., Holtz, H. B., Sweetnam, D. N., Eshleman, V. R. & Tyler, G. L. (1983). The atmosphere of Titan: An analysis of the Voyager 1 radio occultation measurements. *Icarus* **53**, 348-363.

Ott, S. (1991). Analysis of targetting requirements for the Huygens mission. ESTEC Working Paper EWP-1640, 156pp.

Pollack, J. B., Atkinson, D. H., Seiff, A. & Anderson, J. D. (1992). Retrieval of a wind profile from the Galileo Probe telemetry signal. *Space Sci. Rev.* **60**, 143-178.

Smith, P. H., Karkoschka, E. & Lemmon, M. (1992). Titan's North-South asymmetry from HST images. *Bull. Am. Astron. Soc.* **24**, 950.

Smith, P. H., Lemmon, M. T., Lorenz, R. D., Sromovsky, L. R., Caldwell, J. J. & Allison, M. D. (1996). Titan's surface, revealed by HST imaging. *Icarus*, **119**, 336-349.

Smith, P. H., Lemmon, M. T., Caldwell, J. J., Allison, M. D. & Sromovsky, L. R. (1994). HST imaging of Titan. *Bull. Am. Astron. Soc.* **26**, 1181.

Strobel, D. F. & Sicardy, B. (1997). Wind shear and wind gust models. In *Huygens: Science, Payload and Mission*, ESA SP-1177 (this volume).

Toon, O. B., McKay, C. P., Courtin, R. & Ackerman, T. P. (1988). Methane rain on Titan. *Icarus* **75**, 255-284.

Tyler, G. L., Eshleman, V. R., Anderson, J. D., Levy, G. S., Lindal, G. F., Wood, G. E. & Croft, T. A. (1981). Radio science investigations of the Saturn system with Voyager 1: Preliminary results. *Science* **212**, 201-206.